doi:10.26443/seismica.v5i2.1689

SEISMICA

Improving estimates of the b-value in regional catalogs by means of the b-more-positive method

Eugenio Lippiello [1], **Cataldo Godano** * [1], **Giuseppe Petrillo** [2,3]

[1]Department of Mathematics and Physics, Universitá della Campania "L. Vanvitelli" , Viale Lincoln 5, 81100 Caserta, Italy, [2]Earth Observatory of Singapore (EOS), Nanyang Technological University (NTU) 50 Nanyang Ave, Block N2-01a-15, Singapore, [3]CNRS, ENS de Lyon, LPENSL, UMR5672, 69342, Lyon cedex 07, France

Author contributions: *Conceptualization*: Eugenio Lippiello, Cataldo Godano. *Formal analysis*: Eugenio Lippiello, Giuseppe Petrillo. *Writing – original draft*: Eugenio Lippiello.

Abstract The b-value, which controls the slope of the frequency–magnitude distribution of earthquakes, is a critical parameter in seismic forecasting. However, accurately measuring the true b-value is challenging due to the temporal and spatial variations in the completeness of instrumental seismic catalogs. In this study, we systematically compare traditional methods for estimating the b-value with newer approaches, specifically focusing on the b-more-positive estimator based on positive magnitude difference statistics. We conduct this comparison using both synthetic ETAS catalogs, with artificially introduced incompleteness, and instrumental catalogs from five regions: Japan, Italy, Southern California, Northern California, and New Zealand. Our analysis of synthetic ETAS catalogs demonstrates that traditional estimators systematically underestimate the b-value under incompleteness scenarios, whereas the b-more-positive estimator yields highly accurate results. Consistent patterns are found in instrumental catalogs, suggesting that conventional methods also underestimate the b-value in real datasets, with important implications for seismic forecasting. Moreover, the b-more-positive estimator provides robust evidence of significant differences in the b-value across the considered geographic regions.

Production Editor:
Yen Joe Tan
Handling Editor:
György Hetényi
Copy & Layout Editor:
Abhineet Gupta

Received:
April 07, 2025
Accepted:
April 13, 2026
Published:
July 25, 2026

Non-technical summary The b-value measures the ratio of small to large earthquakes and could provide insights into the stress state of fault zones, making it a key tool in earthquake forecasting. However, accurately estimating the b-value is challenging because small earthquakes are often hidden by larger ones or missed due to detection limitations. In this study, we demonstrate that the novel b-more-positive estimator, which expands upon the innovative approach introduced by the b-positive estimator, provides a more reliable b-value calculation. Unlike traditional methods, which systematically underestimate the b-value, the b-more-positive estimator overcomes the challenges of data incompleteness. This conclusion is supported by extensive simulations using synthetic earthquake catalogs, where the impact of incomplete data was deliberately modeled.

1 Introduction

The Gutenberg–Richter (GR) law is a fundamental assumption in most current methods for analyzing earthquake data. It provides essential information, such as the seismicity rate across all event magnitudes in a region, quantified by the exponent of the frequency–magnitude distribution, commonly referred to as the b-value, which typically takes a value around 1 for shallow tectonic events (Frohlich and Davis, 1993).

More specifically, the GR law (Gutenberg and Richter, 1944) states that the probability density $p(m)$ of observing an earthquake with magnitude m is given by

$$p(m) = \beta e^{-\beta(m-m_{\mathrm{L}})}, \quad (1)$$

where β is the scaling parameter, and m_{L} is a minimum reference magnitude. In the following, we report numerical results in terms of β for consistency with the analytical derivations. The corresponding base-10 b-value is obtained as $b = \beta/\ln(10)$.

Variations in the b-value, both spatial and temporal, have been proposed as indicators of several factors influencing seismic regions, including the stress regime, tectonic characteristics, material heterogeneities, and temperature (Tormann et al., 2015; Wiemer and Wyss, 2002; Schorlemmer et al., 2004; Petruccelli et al., 2018; Spada et al., 2013). Laboratory experiments, in particular, have demonstrated an inverse relation between the b-value and differential stress (Scholz, 2015). These findings suggest that the b-value may serve as a stress proxy, potentially aiding in identifying high-stress zones where significant future earthquakes are more likely to occur (Gulia and Wiemer, 2020; Gulia et al., 2020; Lippiello et al., 2025).

Estimating the b-value presents challenges due to the breakdown of exponential decay at lower magni-

*Corresponding author: cataldo.godano@unicampania.it

tudes. This issue arises when cataloging instruments cannot fully capture all earthquakes above background noise, establishing a detection threshold magnitude M_c, where only earthquakes above M_c are detected with 100% probability. However, M_c can fluctuate due to network limitations, such as uneven spatial coverage or sensor variability (Schorlemmer and Woessner, 2008; Mignan et al., 2011; Mignan and Woessner, 2012). Additionally, coda waves from previous, larger events can obscure smaller earthquakes, further influencing M_c and complicating detection (Kagan, 2004; Helmstetter et al., 2006; Peng et al., 2007; Lippiello et al., 2016; Hainzl, 2016a,b; de Arcangelis et al., 2018; Petrillo et al., 2020; Hainzl, 2021). Failure to properly address these factors may lead to a substantial underestimation of the b-value.

To address the issue of incomplete data reporting, the fundamental premise underlying nearly all b-value estimation studies since the introduction of the Maximum Likelihood Estimator (Aki, 1965) is that a reliable b-value can be recovered using the following estimator:

$$\beta_0 = \frac{1}{\langle m \rangle - M_\mathrm{th}}, \tag{2}$$

where $\langle m \rangle$ represents the average magnitude of events exceeding a chosen threshold M_th. In standard practice, researchers first identify the magnitude of completeness M_c and assume that for any $M_\mathrm{th} \geq M_\mathrm{c}$, the magnitude distribution strictly follows an exponential law. This assumption implies that the b-value estimate should remain stable, forming a 'plateau', as M_th increases beyond M_c. The final b-value is then related to the exponential parameter by the relation $b = \beta_0/\ln(10)$.

An innovative approach to this issue was recently introduced by van der Elst (2021) with the development of the 'b-positive' estimator. This method estimates the b-value by analyzing the distribution of magnitude differences, $\delta m = m_{i+1} - m_i$, between consecutive earthquakes in the catalog. Specifically, for a complete dataset that obeys the GR law (Eq. 1), it can be demonstrated that the distribution of δm, denoted as $p(\delta m)$, follows an exponential form with a coefficient $\beta_+ = \beta$. The key insight from van der Elst (2021), validated through extensive numerical simulations, is that when restricting the analysis to positive values of δm, the distribution $p(\delta m)$ is significantly less sensitive to detection issues compared to $p(m)$. Lippiello and Petrillo (2023); Godano et al. (2025) have subsequently demonstrated that accurately identifying the correct b-value from positive magnitude difference statistics necessitates the consideration of additional conditions. Specifically, one can examine the magnitude differences between pairs of earthquakes that are not necessarily consecutive in the catalog. However, it is essential that their epicentral distances are sufficiently small to ensure similar behavior of M_c at their respective epicenters. Under these conditions, which form the basis of the 'b-more-positive' estimator, $p(\delta m)$ is expected to exhibit an exponential decay with a coefficient $\beta_{++} \simeq \beta$, even in the presence of substantial detection issues.

In this study, we will present a detailed comparison of the b-value estimates derived from traditional estimators (Eq. 2) with those obtained using the b-positive estimators, β_+ and β_{++}. We will first conduct this comparison using synthetic ETAS catalogs, where incompleteness is artificially introduced, as outlined in Hainzl (2016a); Petrillo and Lippiello (2020, 2023). The analysis of these synthetic catalogs will provide insights into the behavior of β_0, β_+, and β_{++} when applied to instrumental catalogs from various geographical regions.

2 Magnitude incompleteness

Incomplete earthquake catalogs result primarily from two key factors: seismic network density incompleteness (SNDI) and short-term aftershock incompleteness (STAI). SNDI occurs when it is difficult to detect earthquakes due to a low signal-to-noise ratio. Several factors contribute to this issue, including noise filtering capabilities and, more importantly, the spatial distribution of seismic stations (Mignan and Woessner, 2012). STAI arises from detection limitations in the aftermath of large earthquakes. Smaller aftershocks are often obscured by coda waves generated from prior, larger earthquakes (Lippiello et al., 2019). Empirical observations suggest that STAI can be characterized by a completeness magnitude that decreases logarithmically as a function of the time elapsed since the mainshock (Kagan, 2004; Helmstetter et al., 2006).

Together, SNDI and STAI result in a completeness magnitude $M_\mathrm{c}(t_i, \vec{x_i}, \mathcal{H}_i)$, which depends on the occurrence time t_i, the epicenter coordinates $\vec{x_i}$, and the seismic history $\mathcal{H}_i$ encompassing all previous earthquakes up to time t_i. All earthquakes with magnitudes above M_c are reliably recorded in the catalog but even at the same location $\vec{x_i}$ and for a given seismic history $\mathcal{H}_i$, $M_\mathrm{c}(t_i, \vec{x_i}, \mathcal{H}_i)$ is not uniquely determined. Factors such as diurnal and seasonal variations, staffing changes, and other external influences introduce fluctuations of the order σ around M_c. These fluctuations are typically smaller than the overall spatial and temporal variability of $M_\mathrm{c}(t_i, \vec{x_i}, \mathcal{H}_i)$. The presence of a finite σ affects the detection function $\Phi\left(m - M_\mathrm{c}(t_i, \vec{x_i}, \mathcal{H}_i)\right)$, which denotes the probability that an earthquake with magnitude m, occurring at time t_i and location $\vec{x_i}$, is recorded in the catalog. A common and analytically convenient choice for the detection function is a smooth transition modeled through an error function (Ogata and Katsura, 1993). In this case, the detection probability can be written as:

$$\Phi\left(m - M_\mathrm{c}\left(t_i, \vec{x_i}, \mathcal{H}_i\right)\right) = \frac{1}{2} + \frac{1}{2}\mathrm{Erf}\left(\frac{m - M_\mathrm{c}}{\sigma}\right), \tag{3}$$

where $\mathrm{Erf}(y)$ represents the error function. According to this definition, on average, approximately 98% of earthquakes with $m \geq M_\mathrm{c} + 2\sigma$ are reported. We stress that this functional form represents a reasonable approximation of catalog incompleteness and may not exactly reproduce the empirical detection characteristics of all instrumental catalogs. However, as discussed in the following sections, the efficiency of the proposed method is independent of the specific functional form of Φ.

A number of technical papers provide tools to identify the optimal value of $M_{\rm th}$ such that $M_{\rm th}>M_{\rm c}$ (Mignan and Woessner, 2012). In this study, we focus on three methods: the Maximum Curvature (MAXC) technique (Wiemer and Wyss, 2000), the b-value stability (MBS) method (Cao and Gao, 2002; Woessner and Wiemer, 2005), and the coefficient of variation (CV) method (Godano et al., 2023, 2024). In the MAXC method, $M_{\rm th}$ is defined as the magnitude bin with the highest frequency of events in the non-cumulative frequency–magnitude distribution. The MBS method operates under the assumption that, once the completeness magnitude is exceeded, the estimated b-value converges to a stable plateau for $M_{\rm th}>M_{\rm c}$. In the CV method, $M_{\rm th}$ is identified as the smallest threshold for which the coefficient of variation (the ratio of the standard deviation to the mean value of magnitudes m) exceeds 0.93. These three methods can yield different estimates for $M_{\rm th}$, and thus for β derived from Eq. (2). The resulting values of β based on these thresholds will be denoted as $\beta_{\rm MAXC}$, $\beta_{\rm MBS}$, and $\beta_{\rm CV}$, respectively.

3 Data and methods

3.1 Data

We consider instrumental catalogs from five different seismic regions: Japan, Italy, Southern California, Northern California and New Zealand. For all the catalogs we restrict the analysis to shallow earthquakes (depth smaller than $50\,\rm km$) and magnitudes $m > 0$. For the Japan seismicity we consider the JMA catalog after year 2000 restricting to the mainland. For the Italian seismicity we consider the Horus catalog (Lolli et al., 2020) after 2005, still restricting to the mainland. For Southern California we consider the relocated catalog (Hauksson et al., 2012) from January 1981 to March 2022, for Northern California we consider the relocated catalog (Waldhauser and Schaff, 2008) from January 1984 to December 2021. Finally for New Zealand we take the catalog after 2000. The number of $m > 0$ earthquakes in the five catalogs is reported in Table 1. For Southern and Northern California and New Zealand we considered the local magnitude $m_{\rm L}$ and the JMA magnitude for Japan. For Italy the magnitude adopted is a calibrated conversion relationship between various types of traditional magnitudes and moment magnitude (Lolli et al., 2020). In Fig. 1, we illustrate the spatial distribution of seismicity for the five regions considered in this study.

3.2 The b-more-positive estimator

It is straightforward to show that in the case of two independent random variables, m_i and m_j, distributed according to an exponential law, as in the GR law Eq. (1), the difference $\delta m = |m_i - m_j|$ between any pair of magnitudes m_i and m_j also follows an exponential distribution:

$$p(\delta m) = \frac{1}{2}\beta e^{-\beta \delta m}, \tag{4}$$

where the factor $\frac{1}{2}$ serves as a normalization term, accounting for both possible cases, $m_i > m_j$ and $m_j > m_i$. In the following, we define the quantity

$$\beta_+ = \left(\frac{1}{N_+} \sum_{\substack{i=1 \\ m_j > m_i + \delta M_{\rm th}}}^{N_+} (m_j - m_i - \delta M_{\rm th}) \right)^{-1}, \tag{5}$$

where $j = i+1$ and the sum is restricted only to the N_+ earthquakes m_i that are followed by an earthquake with $m_{i+1} > m_i + \delta M_{\rm th}$. Maximizing the likelihood, under the assumption that Eq. (4) holds (van der Elst, 2021; Gasperini and Tinti, 2023), shows that $\beta_+ = \beta$ up to statistical fluctuations δb of the order of $1/\sqrt{N_+}$.

In the presence of incompleteness, magnitudes no longer obey the GR law, and Eq. (4) must be replaced by the following expression (Lippiello and Petrillo, 2023):

$$p(\delta m) \propto \beta e^{-\beta \delta m} \Phi(m_i + \delta m - M_{\rm c}(t_j, \vec{x}_j, \mathcal{H}_j \,|\, m_i)) \cdot \Phi\left(m_i - M_{\rm c}(t_i, \vec{x}_i, \mathcal{H}_i)\right), \tag{6}$$

where $\Phi\left(m_i - M_{\rm c}(t_i, \vec{x}_i, \mathcal{H}_i)\right)$ is the detection probability as defined in Eq. (3), and $\Phi\left(m_i + \delta m - M_{\rm c}(t_j, \vec{x}_j, \mathcal{H}_j \,|\, m_i)\right)$ represents the detection probability at time t_j and location $\vec{x}_j$, conditional on the previous earthquake m_i being identified and recorded in the catalog. The key insight is that, when the following condition holds:

$$\Phi\left(m_j - M_{\rm c}(t_j, \vec{x}_j, \mathcal{H}_j \,|\, m_i)\right) = 1, \tag{7}$$

then $p(\delta m)$ obeys a pure exponential law with decay controlled by the coefficient β, even if $\Phi\left(m_i - M_{\rm c}(t_i, \vec{x}_i, \mathcal{H}_i)\right) \ll 1$. Let us first consider what happens in the case when $\sigma \to 0$ in Eq. (3), i.e., when the detection function is a discontinuous function changing from $\Phi = 0$ for $m < M_{\rm c}$ to $\Phi = 1$ for $m > M_{\rm c}$. Since m_i has been recorded at time t_i, it is necessary that $m_i \geq M_{\rm c}(t_i, \vec{x}_i, \mathcal{H}_i)$. Consequently, by imposing the constraint $m_j > m_i$ we also have that $m_j \geq M_{\rm c}(t_j, \vec{x}_j, \mathcal{H}_j)$ and Eq. (7) is satisfied provided that the following requirements hold:

Hypothesis (i):

$$M_{\rm c}(t_j, \vec{x}_i, \mathcal{H}_j) \leq \min\{m_i, M_{\rm c}(t_i, \vec{x}_i, \mathcal{H}_i)\}, \tag{8}$$

for $t_j > t_i$.

Hypothesis (ii):

$$M_{\rm c}(t_j, \vec{x}_i, \mathcal{H}_j) = M_{\rm c}(t_j, \vec{x}_j, \mathcal{H}_j). \tag{9}$$

We notice that Eq. (8) is a condition on $M_{\rm c}$ evaluated at the same positions $\vec{x}_i$ but at different times $t_j > t_i$. In contrast, Eq. (9) is a condition at the same time t_j but in different positions $\vec{x}_i$ and $\vec{x}_j$.

Hypothesis (i) is easily satisfied if no earthquake with magnitude greater than m_i occurs within the temporal window (t_i, t_j) between the two earthquakes. Specifically, according to STAI, the obscuration effect caused by earthquakes occurring at times $t < t_i$ diminishes in relevance by the time $t_j > t_i$. Additionally, if all earthquakes in the interval (t_i, t_j) have magnitudes smaller

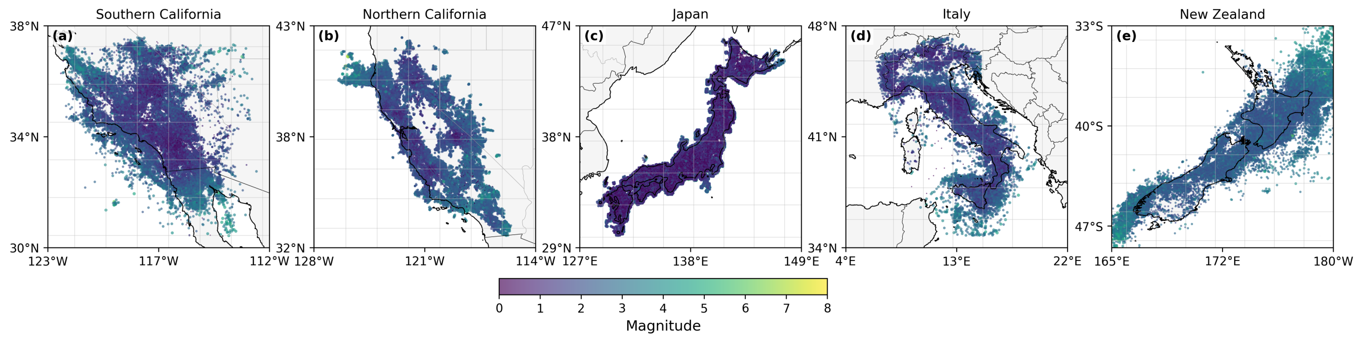

Figure 1 Spatial distribution of seismicity in the five regions considered in this study: (a) Southern California, (b) Northern California, (c) Japan, (d) Italy, and (e) New Zealand. Each point represents an earthquake with magnitude $m > 0$ and depth smaller than $50\,\mathrm{km}$. Colors indicate earthquake magnitude according to the color scale shown below the panels.

than m_i, none of these events can cause a completeness magnitude larger than m_i. More precisely, hypothesis (i) is also met if any $m > m_i$ earthquakes occur within (t_i, t_j) but are sufficiently distant in space so as not to produce obscuration effects at $\vec{x}_j$.

For hypothesis (ii) to hold, it is necessary that the epicentral distance d_{ij} between $\vec{x}_i$ and $\vec{x}_j$ is small enough that the two earthquakes occur in a region with very similar network coverage. Additionally, d_{ij} must be sufficiently small for previous large earthquakes to have comparable obscuration effects at both epicentral positions $\vec{x}_i$ and $\vec{x}_j$. Consequently, for hypothesis (ii) to be valid, an upper bound d_R on d_{ij} must be imposed. The optimal value of d_R depends on the specific spatial configuration of seismic stations and can be associated with the typical distance over which the completeness magnitude M_c can reasonably be considered constant.

Summarizing, in the b-more-positive estimator, we can define a quantity similarly to Eq (5):

$$\beta_{++} = \left(\frac{1}{N_{++}} \sum_{\substack{i=1 \\ m_j > m_i + \delta M_{\mathrm{th}} \\ \& \, d_{ij} < d_R}}^{N_{++}} (m_j - m_i - \delta M_{\mathrm{th}}) \right)^{-1} \tag{10}$$

where j is the index of the closest subsequent earthquake in time that has magnitude $m_j > m_i + \delta M_{\mathrm{th}}$ and an epicentral distance $d_{ij} < d_R$. The sum extends over all N_{++} earthquakes i for which all events recorded in the interval (t_i, t_j) and within an epicentral distance smaller than d_R from $\vec{x}_i$ have magnitudes $m < m_i$. According to the previous arguments, when $\sigma = 0$, we have that $\beta_{++} \simeq \beta$ even in the presence of incomplete datasets also for $\delta M_{\mathrm{th}} = 0$.

In the more realistic case of a finite σ, the detection function grows more smoothly from 0 to 1. Consequently, the fact that m_i has been detected does not automatically imply that $m_i \geq M_c(t_i, \vec{x}_i, \mathcal{H}_i)$. Furthermore, even when $m_j \geq M_c(t_j, \vec{x}_j, \mathcal{H}_j)$, Eq. (7) does not hold automatically, even if conditions (i) and (ii) are satisfied. Nevertheless, since the Erf function is a very steep function that approaches zero for $m_i < M_c - 2\sigma$ and saturates to 1 when $m_i > M_c + \sigma$, one could expect that by imposing $m_j > m_i + \delta M_{\mathrm{th}}$ and choosing $\delta M_{\mathrm{th}} \gtrsim \sigma$, we can be reasonably confident that $m_j \gtrsim M_c(t_j, \vec{x}_j, \mathcal{H}_j) + 2\sigma$. In this case, condition (7) is fulfilled with good accuracy. We wish to remark, however, that the effect of a finite σ introduces a systematic bias, causing β_{++} to be smaller than β_{true}. Indeed, for a finite detection function, it is more probable to miss earthquake pairs with a smaller magnitude difference $m_j - m_i$. The effect of a finite σ can be studied numerically; in Appendix A, we show that the data are consistent with the expression:

$$\beta_{++} = \beta_{\mathrm{true}} \left(1 - \epsilon \frac{\delta M_{\mathrm{th}}}{\sigma} \right) \tag{11}$$

with $\epsilon(x) \simeq 0.2\beta^2\sigma^2(x+1)10^{-x}$. This result demonstrates that β_{++} approaches β_{true} as soon as $\delta M_{\mathrm{th}} \gg \sigma$. In particular, we find that $\epsilon \lesssim 0.01$ when $\delta M_{\mathrm{th}} = 2\sigma$, which represents an approximation error smaller than the typical uncertainty in the β evaluation caused by statistical fluctuations.

The algorithm implementing the b-more-positive estimator β_{++} presents the following scheme:

For all earthquakes i in the catalog:

1. Search forward in time through subsequent earthquakes j until you find the first one that satisfies both conditions $m_j > m_i$ and $d_{ij} < d_R$;
2. If $m_j \geq m_i + \delta M_{\mathrm{th}}$, add $(m_j - m_i - \delta M_{\mathrm{th}})$ to the sum in Eq. (10) and count i toward N_{++}, then move to the next i;
3. If $m_i < m_j < m_i + \delta M_{\mathrm{th}}$, do not include $(m_j - m_i + \delta M_{\mathrm{th}})$ in the summation of Eq. (10), and proceed directly to the subsequent earthquake $i+1$.

For each i, the search stops at the first j fulfilling step (a).

The b-positive estimator represents a specific case of the b-more-positive estimator in which the index j considers only the subsequent earthquake, specifically $j = i+1$, with the condition $d_R = \infty$.

4 Results

4.1 The evaluation of the b-value in synthetic ETAS catalogs

The Epidemic–Type Aftershock Sequence (ETAS) model effectively captures the main characteristics

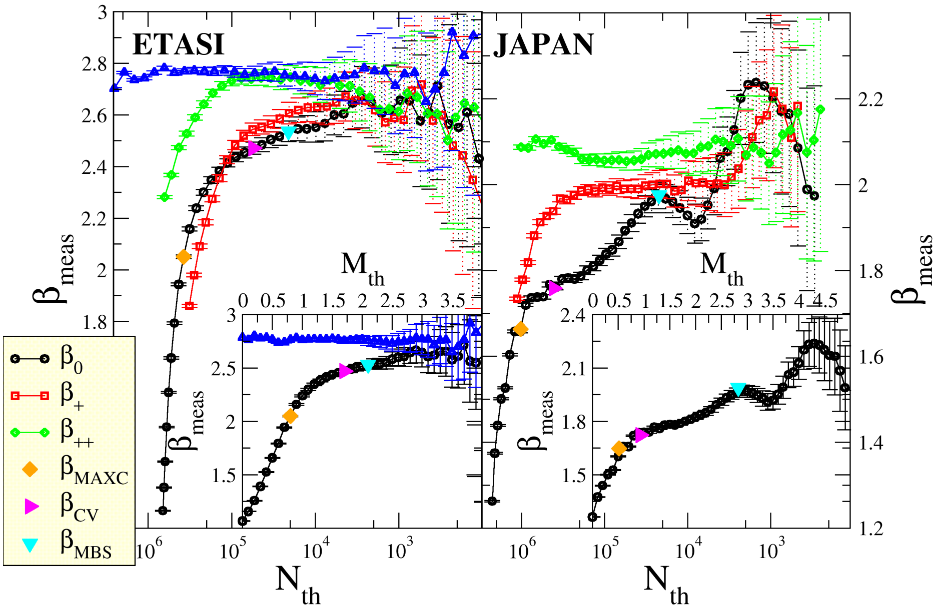

Figure 2 (Main Panels) The value of β (corresponding to $b = \beta/\ln(10)$) measured using the three estimators, β_0, β_+, and β_{++}, is shown as a function of $N_{\rm th}$ in a synthetic ETASI catalog (main left panel) and in the JMA catalog for Japan (main right panel). Black, red, and green symbols are used for β_0, β_+, and β_{++}, respectively. The values for $\beta_{\rm MAXC}$, $\beta_{\rm CV}$, and $\beta_{\rm MBS}$ are marked by a filled orange diamond, a magenta right triangle, and a cyan downward triangle, respectively. Error bars represent twice the standard deviation. For clarity, only in left panels, blue upward triangles denote results from the β_0 estimator applied to the complete ETAS catalog. (Insets) β_0 for the ETASI catalog (left panel) and for the JMA catalog (right panel), along with the three estimates $\beta_{\rm MAXC}$, $\beta_{\rm CV}$, and $\beta_{\rm MBS}$, is plotted as a function of $M_{\rm th}$. In the inset of the left panel, we also plot results for β_0 for the complete ETAS catalog.

of the spatio-temporal evolution of seismicity (Ogata, 1988, 1998) and is widely regarded as the benchmark for earthquake forecasting (Lombardi and Marzocchi, 2010; Nandan et al., 2019). In this study, synthetic earthquake catalogs are generated using the ETAS model (Ogata, 1989; Zhuang and Ogata, 2006). The simulation starts with background events from a Poisson process and recursively adds triggered events according to the productivity law, Omori–Utsu temporal decay (Omori, 1894), the power law decay of the distribution of epicentral distances (LIPPIELLO et al., 2009) and the GR magnitude distribution (Gutenberg and Richter, 1944). To be more precise, the simulation starts with a set of background events (zero-th generation) from a Poisson process in time and spatially distributed to reflect the heterogeneous pattern of epicentral distribution in instrumental data sets. Each event generates a number of offspring according to a Poisson distribution with mean productivity depending on the event magnitude and occurrence time. The magnitudes of the offspring follow the GR distribution and the occurrence times and spatial distances are drawn from the empirical probability densities. Only events within the simulation time window are retained, and the process is iterated over successive generations until no new events occur within the window. This approach ensures that the synthetic catalogs reproduce both the temporal, spatial, and magnitude statistics of real ETAS sequences. Details can be found in de Arcangelis et al. (2016). The key assumption of the ETAS model is that magnitudes are independent variables drawn from the GR law with a β value. Deviations from the GR law, caused by catalog incompleteness, can be incorporated into the model following the scheme outlined in de Arcangelis et al. (2018); Petrillo and Lippiello (2020, 2023). More precisely, STAI can be implemented by considering a constant blind time τ (Hainzl, 2016a,b, 2021). For any earthquake j in the original complete catalog, we consider all events with magnitude m_i that occurred in the previous time interval $t_i \in (t_j - \tau, t_j)$ and within an epicentral distance $d_{ij} < 50\,\mathrm{km}$. Each event j is then removed from the catalog with a probability $\Phi(m_i - m_j)$, where $\Phi(x)$ is defined in Eq (3) with $\sigma = 0.4$. This procedure corresponds to a history–dependent probabilistic thinning of the complete ETAS catalog, where each event is retained with a probability determined by the magnitude of preceding earthquakes within a prescribed space–time window (e.g., Ogata, 1981). It is possible to show that the presence of a constant blind time leads to a completeness magnitude decreasing logarithmically in time consistently with instrumental observations (Hainzl, 2016a,b).

To incorporate SNDI, we impose an additional spatially variable baseline detection threshold, meant to reproduce the heterogeneity in catalog completeness caused by the non-uniform geometry of the seismic network. Specifically, we adopt the spatial dependence of the completeness magnitude estimated by Schorlemmer and Woessner (2008) for Southern California, and denote by $m_r(\vec{x})$ the corresponding local reference threshold at position $\vec{x}$. Then, after applying the STAI thinning described above, an event of magnitude m_i in the catalog is further removed with probability $1 - \Phi(m_i - m_r(\vec{x}_i))$, where $\vec{x}_i$ is the epicentral position of the event, and Φ is the same detection function defined in Eq. (3) with $\sigma = 0.4$. In this way, earthquakes occurring in areas characterized by poorer station coverage, and thus by larger values of $m_r(x)$, have a higher probability of being missed, whereas events in better-instrumented areas are preferentially retained.

The ETAS model incorporating only STAI is commonly referred to in the literature as the Incomplete ETAS (ETASI) model (de Arcangelis et al., 2018). van der Elst (2021) utilized this model to simulate single mainshock–aftershock sequences, demonstrating the efficacy of the b-positive method in recovering correct b-values despite STAI effects. Subsequently, Lippiello and Petrillo (2023) generated synthetic ETASI catalogs containing multiple sequences, reaching similar conclusions for the b-more-positive estimator. Lippiello and Petrillo (2023) also investigated synthetic catalogs affected solely by SNDI, highlighting the limitations of the b-positive method and the superior efficiency of the b-more-positive estimator. In the present study, we investigate the simultaneous presence of both STAI and SNDI within ETAS catalogs. Hereafter, we will continue to use the term "ETASI catalogs" to refer to synthetic datasets featuring both STAI and SNDI. We generate synthetic ETASI catalogs containing earthquakes with $m_i > 0$, over a period of 25 years. The key quantity in our analysis is β_{true}, and we consider different values of $\beta_{\text{true}} \in [2, 3]$. For each value of β_{true}, we generate up to ten different synthetic catalogs, each obtained by implementing a different random seed. The values of the other parameters in the ETASI model are not relevant to the present study, and we adopt those parameters optimized for Southern California, as detailed in Petrillo and Lippiello (2020). In the synthetic ETAS catalogs, the β_{true} value is the exact parameter imposed in the simulation. This value is used as the "prior" reference for evaluating the bias of the different estimators. In our simulations we focus on results for a b-value of $b = 1.2$, corresponding to $\beta_{\text{true}} = 2.763$, though similar observations hold for other choices of β_{true}. We always start from an original dataset containing $N_T \in [5 \times 10^6, 1 \times 10^7]$ earthquakes with $m_i > 0$. After applying STAI, about 70–80% of earthquakes are removed. Another significant removal is obtained to implement SNDI, obtaining final ETASI catalogs with $N_T \in [3 \times 10^5, 9 \times 10^5]$ $m > 0$ events, which is comparable with the number observed in instrumental catalogs.

In Fig. 2, we plot results for a specific synthetic ETAS catalog, which initially contains 9 961 297 m>0 earthquakes, reduced to 2 142 912 after STAI and to 668 284 after SNDI; similar patterns are observed for other synthetic catalogs. We show results for the quantity β_0 evaluated in the original complete catalog, which provides the reference curve for the true β value, β_{true}. This value is compared with the values of β (β_{meas}) measured in the final incomplete catalog, obtained using the three estimators β_0 (Eq. 2) for different values of M_{th}, β_+ (Eq. 5), and β_{++} (Eq. 10), both evaluated at different values of δM_{th}. By increasing M_{th} and δM_{th}, we reduce the number of earthquakes N_{th} used for the three estimators. More precisely, N_{th} represents the number of earthquakes with $m > M_{\text{th}}$ in the evaluation of β_0 (Eq. 2), $N_{\text{th}} = N_+$ in the evaluation of β_+ (Eq. 5), and $N_{\text{th}} = N_{++}$ in the evaluation of β_{++} (Eq. 10). We plot the data as a function of N_{th} to allow a direct comparison among the different estimators. Furthermore, since the standard deviation $\delta\beta$ in all three estimators is approximately $\beta_{\text{meas}}/\sqrt{N_{\text{th}}}$, this plot allows us to identify the best estimator as the one that, for fixed N_{th}, better approximates β_{true}. More specifically, we use $\delta\beta$ for the standard deviation in each estimator, obtained by Tinti and Mulargia (1987) for the b-value and by Gasperini and Tinti (2023) for the b-positive estimator. In the figure, we display $2\delta\beta$ as error bars to represent this uncertainty. We specify that the expression for the standard deviation is derived under the assumption that magnitudes are independent and identically distributed variables. This hypothesis is widely accepted in the literature, even in the presence of strong temporal and spatial clustering of seismic events. To associate each point of the curve with its corresponding δM_{th} value, we specify that δM_{th} is monotonically increased in the range $[0, 2]$ with constant increments of 0.1. Consequently, the k-th point (ordered from left to right) on the β_+ and β_{++} curves corresponds to a threshold value of $\delta M_{\text{th}} = 0.1k$.

In the inset of Fig. 2 (left panel), we plot β_0 for both the complete and incomplete catalogs as a function of M_{th}, finding that β_0 significantly underestimates β_{true} in the incomplete catalog. In fact, in the incomplete catalog, β_0 grows as a function of M_{th} but remains consistently below β_{true}. The downward bias observed in our synthetic tests (Fig. 2) stems from the joint action of STAI and SNDI: (i) STAI yields an elevated, time dependent $M_c(t)$ after large events, so that moderate thresholds M_{th} still mix complete and incomplete portions of the catalog; (ii) SNDI imposes a spatially varying baseline $M_c(\vec{x})$ tied to station coverage. Consequently, heuristic completeness picks may identify early plateaus in $\beta_0(M_{\text{th}})$ that are in fact pre-asymptotic with respect to STAI, thus underestimating b. A reasonable estimate of β_{true} can only be achieved at very large values of M_{th}, where, however, the uncertainty becomes substantial ($\delta\beta \approx 0.3$) due to the reduced number N_{th}. The fact that the β_0 curve grows monotonically across the entire explored M_{th} range, while remaining systematically below β_{true}, indicates that traditional estimators inherently underestimate the true β value, regardless of the specific estimator employed. Indeed, all three traditional estimates — β_{MAXC}, β_{MBS}, and β_{CV} — yield values significantly smaller than β_{true}. This behavior is observed not only for the specific synthetic ETAS catalog shown in Fig. 2, but also across the other nine synthetic catalogs generated with the same β_{true}, as well as for additional catalogs characterized by different β_{true} values.

Fig. 2 also shows that β_+ underestimates β_{true} across

Catalog	N	β_{MAXC}	β_{CV}	β_{MBS}	$\beta_{++}^{\max}$	$\overline{\beta_{++}}$	$\beta_{+}^{\max}$
Instrumental Catalogs							
Japan	2 313 836	1.658 ± 0.006	1.74 ± 0.01	1.96 ± 0.05	2.11 ± 0.01	2.08 ± 0.02	2.00 ± 0.05
Southern California	794 838	1.63 ± 0.01	2.18 ± 0.02	2.34 ± 0.04	2.44 ± 0.04	2.41 ± 0.06	2.27 ± 0.05
Northern California	856 142	1.48 ± 0.01	2.08 ± 0.03	2.22 ± 0.02	2.29 ± 0.02	2.28 ± 0.02	2.35 ± 0.06
Italy	363 936	1.89 ± 0.02	2.16 ± 0.03	2.33 ± 0.08	2.63 ± 0.02	2.59 ± 0.03	2.32 ± 0.04
New Zealand	165 714	1.84 ± 0.02	1.91 ± 0.02	2.01 ± 0.03	2.53 ± 0.02	2.45 ± 0.05	2.20 ± 0.03
Synthetic ETASI catalogs $\beta_{\mathrm{true}} = 2.763$							
ETASI 1	668 284	1.986 ± 0.006	2.078 ± 0.006	2.53 ± 0.04	2.71 ± 0.02		2.63 ± 0.02
ETASI 2	641 320	1.942 ± 0.006	2.036 ± 0.006	2.57 ± 0.05	2.73 ± 0.02		2.66 ± 0.02
ETASI 3	722 492	2.103 ± 0.006	2.178 ± 0.008	2.55 ± 0.03	2.74 ± 0.02		2.64 ± 0.02
ETASI 4	305 887	2.26 ± 0.01	2.26 ± 0.01	2.68 ± 0.07	2.75 ± 0.03		2.70 ± 0.02
ETASI 5	730 056	2.049 ± 0.006	2.153 ± 0.006	2.53 ± 0.03	2.71 ± 0.03		2.62 ± 0.02
ETASI 6	432 091	2.131 ± 0.008	2.131 ± 0.008	2.57 ± 0.06	2.74 ± 0.03		2.67 ± 0.02
ETASI 7	840 102	1.968 ± 0.006	2.043 ± 0.006	2.60 ± 0.08	2.73 ± 0.02		2.67 ± 0.02
ETASI 8	346 611	1.964 ± 0.006	2.051 ± 0.006	2.55 ± 0.05	2.73 ± 0.03		2.64 ± 0.02
ETASI 9	335 283	2.215 ± 0.008	2.215 ± 0.008	2.75 ± 0.12	2.75 ± 0.03		2.71 ± 0.02
ETASI 10	646 730	2.049 ± 0.006	2.131 ± 0.007	2.52 ± 0.04	2.73 ± 0.02		2.61 ± 0.02

Table 1 Comparison of different estimators for the β value across five geographic regions and for ten different realizations of the ETASI catalog, with $\beta_{\mathrm{true}} = 2.763$ and $d_R = 40\,\mathrm{km}$ implemented. We do not report $\overline{\beta_{++}}$ in ETASI catalogs since it coincides with $\beta_{++}^{\max}$. All reported values correspond to $\beta = b\ln(10)$ (i.e., $b = \beta/\ln(10)$). N is the total number of $m > 0$ earthquakes in each catalog.

all values of N_+, except at very large $\delta M_{\mathrm{th}} > 3.8$, where $N_+ \approx 100$ and fluctuations become large enough to encompass β_{true}. Interestingly, Fig. 2 reveals that β_{++} provides a sufficiently accurate estimate of β_{true} already for $N_{++} > 10^5$ (when $\delta M_{\mathrm{th}} = 0.8$). This confirms that, within the tested ETASI incompleteness model, the b-more-positive estimator effectively recovers the imposed b-value. More specifically, we observe that β_{++} initially underestimates the true β value when $\delta M_{\mathrm{th}} = 0$, then increases monotonically up to $\delta M_{\mathrm{th}} = 0.8$, and subsequently remains approximately constant for larger values of δM_{th}.

Following the rationale behind the MBS methodology, we can define the best estimate $\beta_{++}^{\max}$ from β_{++} as the value obtained from Eq (10) for the first value of δM_{th} such that $\Delta\beta = |\beta_{\mathrm{ave}} - \beta_{++}| \leq \delta\beta_{++}$. Here, $\delta\beta_{++}$ represents the standard deviation of β_{++}, and β_{ave} is the average value of β_{++} over five successive cutoff magnitudes δM_{th}, with δM_{th} incremented by 0.1 in each step. Results for $\beta_{++}^{\max}$ are provided in Tab. 1 for the 10 synthetic ETASI catalogs, showing substantial agreement with β_{true} despite a slight underestimation.

4.2 The evaluation of the b-value regional catalogs

In instrumental catalogs, magnitudes are reported with a fixed resolution of 0.1 units. This binning introduces a systematic underestimation of the b-value when using Eq. (2), because the discrete nature of the data biases the mean magnitude upward. The bias becomes even more pronounced when using the b-positive and b-more-positive estimators. Analytical corrections to address this issue have been proposed by van der Elst (2021) and Gasperini and Tinti (2023). A different strategy (cf., Godano et al., 2014; Lippiello and Petrillo, 2023) consists in introducing a small random perturbation, uniformly distributed in the interval $(-0.05, 0.05)$, to each magnitude in the catalog. As shown in Appendix B, this procedure effectively compensates for the rounding effect and yields an accurate estimate of the b-value. We have explicitly verified that the results presented in this study remain substantially identical regardless of the magnitude rounding strategy, confirming that our findings are robust against rounding effects. Finally, we observe that no specific procedures were implemented to remove quarry blasts or induced seismicity events from the five regional catalogs.

4.2.1 The b-value in the JMA catalog

Results for the JMA catalog are plotted in the right panel of Fig. 2. The behavior of β_0 is similar to that observed in the ETASI catalog (left panel). Specifically, we see that β_0 increases with M_{th}, reaching an initial plateau at $\beta_{\mathrm{CV}} = 1.74 \pm 0.01$. With further increases in M_{th}, β_0 resumes its growth, eventually stabilizing at a value close to $\beta_{\mathrm{MBS}} = 1.96 \pm 0.05$. For even larger M_{th} values, β_0 shows additional growth toward $\beta \gtrsim 2.1$, albeit with an uncertainty of approximately $\delta\beta \simeq 0.15$.

In contrast, the quantity β_+ quickly stabilizes at a plateau value around β_{MBS} and remains nearly constant across all values of δM_{th}. Meanwhile, β_{++} transitions from an initial value of $\beta_{++} = 2.06 \pm 0.01$ at $\delta M_{\mathrm{th}} = 0$ to $\beta_{++} = 2.11 \pm 0.01$ at $\delta M_{\mathrm{th}} = 0.4$, after which it decreases slightly to approximately $\beta_{++} = 2.07 \pm 0.01$.

The comparison with Fig. 2 highlights that the value of β estimated from β_0 tends to be underestimated. Specifically, we find $\beta_{\mathrm{MBS}} = 1.96 \pm 0.05$, which should be compared to $\beta_{++}^{\max} = 2.11 \pm 0.01$. This latter value, $\beta_{++}^{\max}$, is expected to be less affected by incompleteness under the stated assumptions and therefore provides a

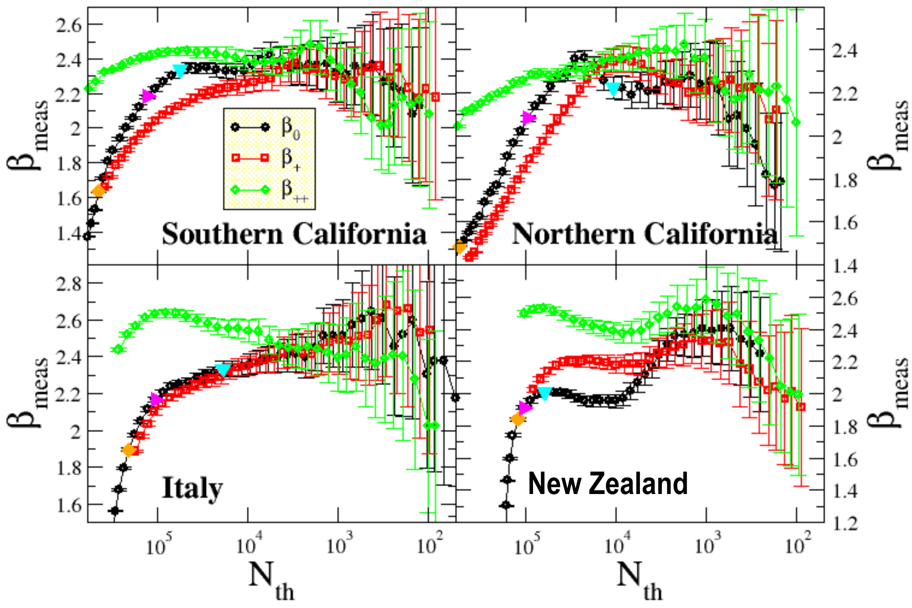

Figure 3 The values of β (corresponding to $b = \beta/\ln(10)$), measured using the three estimators β_0, β_+, and β_{++}, are plotted as functions of N_{th} for the four geographic regions: Southern California (upper left panel), Northern California (upper right panel), Italy (lower left panel) and New Zealand (lower right panel). Error bars represent twice the standard deviation, and the same colors and symbols as in Fig. 2, also for the quantities β_{MAXC}, β_{CV}, and β_{MBS}, are used for consistency.

more robust estimate of the b-value.

4.2.2 The b-value in the Italian, Southern, Northern and New Zealand catalogs

The values of β_0, β_+, and β_{++} as functions of N_{th} for the remaining four geographic regions are shown in Fig. 3. In all cases, β_0 starts from very low values at large N_{th} and eventually stabilizes in an intermediate regime, roughly constant, meeting the criteria necessary for identifying M_c in the MAXC, CV and MBS methods.

As N_{th} decreases further, distinct behaviors emerge across the regions: in Italy, β_0 continues to increase gradually; in Southern California, it remains approximately stable; while in Northern California and New Zealand, it appears to decline. It is worth noting that in this low-N_{th} regime, statistical fluctuations become significant, and the observed trends may simply reflect random variability rather than a meaningful pattern.

In all four regions, we consistently find that β_0 is significantly lower than β_{++} at large N_{th}, aligning with findings from the synthetic ETASI catalog and the results previously observed for Japan (Fig. 2). Fig. 3 indicates that, in the regional catalogs analyzed here, the traditional estimator β_0 provides systematically smaller values than β_{++}. The values for β_{MAXC}, β_{MBS}, β_{CV}, and $\beta_{++}^{\max}$, along with their associated uncertainties, are presented in Tab. 1 for all five geographic regions. We also present the value of $\beta_{+}^{\max}$ defined as the value provided by the MBS method when considering the β_+ vs δM_{th} curve.

Results of Fig. 3 are obtained using d_R= 40 km, for the constraint on the maximum pairwise distance used in the evaluation of β_{++}. The same analysis is repeated in Appendix C and indicates that the b-value estimate remains robust and stable for $d_R < 90$ km.

5 Discussion

The completeness magnitude M_c exhibits significant spatio-temporal variations. Spatial fluctuations are primarily driven by the non-uniform coverage of the seismic network, while temporal changes are largely dictated by STAI effect, where the coda waves of large earthquakes obscure subsequent smaller events. A precise, real-time evaluation of M_c at any specific location is practically unfeasible, as it would require exact knowledge of the wave propagation from all preceding events to determine if a signal of a given amplitude is detectable. The primary advantage of the b-positive framework is that the value of $M_c(t, \vec{x}, \mathcal{H})$ becomes irrelevant. The core principle is that if an earthquake with magnitude m_i is detected, it implies $m_i > M_c$. Consequently, for any subsequent event with $m_j > m_i$, the condition $m_j > M_c$ is also satisfied, ensuring that both events are recorded. However, for this condition to hold, two requirements must be met:

1. No event larger than m_i must occur between m_i and m_j;
2. The events must occur sufficiently close in space so that the network's detection probability remains the same at both epicenters.

This second condition, implemented by imposing $d_{ij} < d_R$, represents the fundamental advancement of the b-more-positive estimator over the original b-positive one. This spatial constraint is essential for effectively managing the spatial heterogeneity of M_c.

In addition to the distance parameter d_R, the b-more-positive method depends on the threshold parameter $\delta M_{\rm th}$. This parameter is introduced to compensate for the fact that the detection function transitions from zero to one over a magnitude range of approximately 2σ. In this study, we evaluated the bias induced by a finite σ on β_{++} and found that for $\delta M_{\rm th} > 2\sigma$, the correction is typically below $2\,\%$.

The optimal values for these two parameters can be determined by identifying the maximum d_R and the minimum $\delta M_{\rm th}$ at which β_{++} becomes independent of their further variation. We observe that these conditions are reasonably satisfied by setting $d_R \simeq 40\,{\rm km}$ and $\delta M_{\rm th} \simeq 0.8$.

Nevertheless, results obtained from regional catalogs exhibit some discrepancies compared to the expected theoretical behavior. A detailed analysis across different regional catalogs (Figs. 2 and 3) reveals a non-monotonic variation in β_{++} as a function of $\delta M_{\rm th}$ (or, equivalently, as a function of the decreasing number of events $N_{\rm th}$). Specifically, β_{++} initially increases from $\delta M_{\rm th} = 0$, reaching a peak value $\beta_{++}^{\max}$ near $\delta M_{\rm th} = 0.5$, followed by a gradual decline as $\delta M_{\rm th}$ further increases. This downward trend is particularly evident in Italy and even more pronounced in New Zealand. In the Italian catalog, β_{++} decreases from a peak $\beta_{++}^{\max} = 2.64 \pm 0.02$ at $\delta M_{\rm th} = 0.5$ to $\beta_{++}^{\min} = 2.55 \pm 0.03$ at $\delta M_{\rm th} = 1.2$. Similarly, in New Zealand, β_{++} declines from $\beta_{++}^{\max} = 2.68 \pm 0.02$ at $\delta M_{\rm th} = 0.3$ to $\beta_{++}^{\min} = 2.53 \pm 0.03$ at $\delta M_{\rm th} = 1.1$. A similar, though less marked, decline is observed in Japan and Southern California, whereas it is absent in Northern California.

The initial increase in β_{++} with increasing $\delta M_{\rm th}$ aligns with theoretical predictions (Sec. 3.2) and is reproduced in synthetic ETASI catalogs (Fig. 2). However, the subsequent decrease was unexpected and may indicate distinctive features of real seismicity not fully captured by the ETASI model. A validation test presented in Appendix D suggests that, at least for Japan and New Zealand, this non-monotonic behavior represents a genuine pattern. To account for the non-monotonic behavior of β_{++} as a function of $\delta M_{\rm th}$, Tab. 1 reports the maximum value $\beta_{++}^{\max}$ for each of the five regions, alongside $\overline{\beta_{++}}$, which represents the mean value calculated between $\beta_{++}^{\max}$ and the minimum value $\beta_{++}^{\min}$ observed within the investigated range of $\delta M_{\rm th}$. The results presented in Tab. 1 demonstrate that both the value of $\beta_{++}^{\max}$ and $\overline{\beta_{++}}$ is significantly larger than the β value obtained with traditional estimators or with β_+. The only exception is represented by Northern California where $\beta_{+}^{\max} > \beta_{++}^{\max}$. In Appendix D we present a statistical test to establish the significance of the observed difference between $\beta_{++}^{\max}$ and $\beta_{++}^{\min}$. We find that the hypothesis of a significant decrease in β_{++}, corresponding to a significant difference between $\beta_{++}^{\max}$ and $\beta_{++}^{\min}$, can be accepted with a confidence level greater than $95\,\%$ for three regions (Japan, Italy, and New Zealand).

At present, we do not have an interpretation for the decrease of β_{++} at large $\delta M_{\rm th}$, which must therefore be associated with aspects of real seismicity that are not accounted for by the ETASI model. One possible explanation concerns our assumption of a single b-value across the entire simulated region. In light of the differences observed in our study among the five regions, it would likely be more realistic to consider a spatially variable b-value. The possibility that such spatial heterogeneity is responsible for the non-monotonic behavior could be tested by performing the analysis on smaller subregions within each regional catalog. Nevertheless, this procedure would reduce the available dataset, thereby increasing statistical uncertainty and making it more difficult to disentangle genuine seismic patterns from random fluctuations. One alternative explanation could involve intrinsic correlations between earthquake magnitudes, which the ETAS model does not account for (Petrillo and Zhuang, 2022, 2023). A fundamental assumption of the ETAS model is that magnitudes are independent and identically distributed. Yet, recent studies, focusing on positive magnitude differences that are less affected by incompleteness, have revealed significant magnitude correlations (Lippiello et al., 2024). These correlations suggest that a single β value may be insufficient to fully characterize the distribution. For example, Nandan et al. (2019, 2022) proposed a modified ETAS model incorporating two distinct β values for aftershocks, based on the magnitude of the triggering mainshock. Similarly, studies such as (Lippiello et al., 2007, 2008) have suggested that the magnitude distribution might also depend on the time interval between triggered and triggering earthquakes. This view aligns with empirical observations of a temporary increase in β following large earthquakes, with a gradual return to a baseline β value over time (Gulia et al., 2016; Gulia and Wiemer, 2020). In a simpler framework, an ETAS model with two distinct β values – one for triggered events and another for background seismicity – could plausibly explain the observed decrease in β_{++} at higher $\delta M_{\rm th}$ values.

Finally, we emphasize that all our b-value estimates are obtained from regional catalogs without applying any declustering. In fact, declustering routines remove events from the catalog, which directly violates the requirement that the pair (m_i, m_j) must be "consecutive" (i.e., no event $m_k > m_i$ occurs between them within distance d_R). Consequently, filtering a catalog through declustering severely undermines the performance of both b-positive and b-more-positive estimators.

6 Conclusions

We have estimated the b-value in synthetic ETAS catalogs after the removal of small-magnitude earthquakes to account for STAI and SNDI. Our findings demonstrate that traditional methods, which rely on identifying a magnitude threshold $M_{\rm th}$ above the completeness level and fitting a GR law for magnitudes $m > M_{\rm th}$, systematically underestimate the true b-value. In contrast, we show that the b-more-positive estimator, β_{++}, provides an accurate and robust estimate of the true b-

value. Additional analyses on the effects of magnitude rounding and finite uncertainty σ, which further support these conclusions, are presented in Appendices A and B; these investigations were partly motivated by the reviewers' comments, and further details can be found in the associated review–response document available online.

While the proposed approach shows high efficiency in synthetic catalogs and effectively removes biases associated with STAI and SNDI, some caution is required when applying it to real instrumental catalogs. In particular, as for other methods proposed in the literature, performance may degrade in the presence of measurement uncertainties, and catalog heterogeneities, potentially leading to residual biases that are not fully filtered by the method. Therefore, applications to small or imperfect datasets should be interpreted with care. Our results on instrumental catalogs show that β_{++} consistently yields higher values than traditional estimators. This implies that conventional b-value estimates used in many seismic forecasting studies are biased low. Provided that the other parameters of the forecasting model remain unchanged, such a bias may have led to a systematic overestimation of seismic hazard. Correcting this bias is therefore of primary importance for improving the reliability of seismic forecasting models.

A further novel result of our study is that β_{++} reveals significant differences in the b-value across the five considered regions. This challenges the common assumption of a region–independent b-value and opens the way to a more realistic description of seismicity that explicitly incorporates regional variability.

In addition, β_{++} exhibits a gradual but significant decrease with increasing $\delta M_{\rm th}$, a feature not reproduced in incomplete ETAS catalogs. This behavior may reflect genuine deviations from the GR law, potentially related to recently identified correlations between earthquake magnitudes and/or spatial variation of the b-value. Disentangling whether this trend arises from statistical fluctuations or reflects intrinsic properties of seismicity remains a critical challenge, with direct implications for refining earthquake forecasting.

Future studies could extend our analysis to smaller subregions within each catalog, in order to better resolve local spatial variations of the b-value inside each geographic region. Such work would further clarify the physical origin of regional differences and provide a stronger basis for the development of next-generation seismic forecasting models.

Acknowledgements

E.L. acknowledges support from the MIUR PRIN 2022 PNRR P202247YKL, C.G. acknowledges support from the MIUR PRIN 2022 PNRR P20222B5P9.

Data availability statement

Instrumental earthquake catalogs can be accessed online through the following links: **Japan**: https://www.data.jma.go.jp/eqev/data/bulletin/index.html, **Southern California**: https://scedc.caltech.edu/data/alt-2011-dd-hauksson-yang-shearer.html, **Northern California**: https://ncedc.org/ncedc/catalog-search.html, **Italy**: https://horus.bo.ingv.it/, and **New Zealand**: https://quakesearch.geonet.org.nz/. In addition, tools for generating synthetic ETASI catalogs are available at https://doi.org/10.5281/zenodo.18831071.

Appendix A: Robustness of the β_{++} framework and finite detection uncertainty

The robustness of the β_{++} framework relies on the functional form of the detection probability $\Phi(m - M_{\rm c})$. As a general property, it is reasonable to expect that the detection probability is characterized by a rapid transition: it saturates to unity for $m > M_{\rm c} + \sigma$ and decays to zero for $m < M_{\rm c} - \sigma$, where σ defines the scale of the detection uncertainty.

Given a detected magnitude m_i, the probability that a subsequent event m_j (with $m_j > m_i + \delta M_{\rm th}$) is missed by the catalog can be formally expressed as:

$$\begin{aligned} &P(\text{not detected} \mid m_j > m_i + \delta M_{\rm th}) \\ &\quad = 1 - \frac{\int_{m_i+\delta M_{\rm th}}^{\infty} \Phi(m - M_{\rm c}) p(m)\, dm}{\int_{m_i+\delta M_{\rm th}}^{\infty} p(m)\, dm} \end{aligned} \tag{12}$$

where $p(m)$ represents the true underlying magnitude distribution (Eq. 1). It is evident that $P(\text{not detected} \mid m_j > m_i + \delta M_{\rm th}) \to 0$ as $\delta M_{\rm th}$ becomes significantly larger than σ, vanishing exactly only in the limit $\delta M_{\rm th}/\sigma \to \infty$. In this appendix, we explore the systematic error introduced by a finite value of $\delta M_{\rm th}/\sigma$.

We first observe that the detection probability is an increasing function of magnitude, which introduces a systematic bias in the calculation of β_{++}. Specifically, it is more probable to miss earthquake pairs characterized by a smaller difference $m_j - m_i$. Consequently, the first detected event m_j used in the evaluation of β_{++} (Eq. 10) will be, on average, larger than the corresponding event in a complete dataset. This leads to a systematic bias $\epsilon = (\beta_{\rm true}/\beta_{++}) - 1 > 0$, which vanishes only in the limit $\delta M_{\rm th}/\sigma \to \infty$.

To quantify this bias, we model the detection function Φ using an error function (Eq. 3) to account for the Gaussian distribution of the detection threshold. Since Eq. (12) lacks a closed-form analytical solution when involving the error function, we evaluate the bias through numerical simulations using the following procedure:

1. **Selection of m_i**: We extract a magnitude m_i from the GR law with a given β. The event is accepted with probability $\Phi(m_i - M_{\rm c})$. If rejected, the process is repeated until a value is accepted.

2. **Comparison of Datasets**:

   (a) For the *complete dataset*, we extract subsequent magnitudes m_2, from a GR law with the same β, until the condition $m_2 > m_i + \delta M_{\rm th}$ is met. We then store the value $\Delta m^{\rm compl} = m_2 - m_i - \delta M_{\rm th}$.

(b) For the *incomplete dataset*, we further require that the selected m_2 be accepted with probability $\Phi(m_2 - M_c)$. If it is accepted we store the value $\Delta m^{\text{uncompl}} = m_2 - m_i - \delta M_{\text{th}}$. Conversely, if m_2 is rejected by the detection function, new values of m_2 are extracted until both the threshold condition ($m_2 > m_i + \delta M_{\text{th}}$) and the detection condition are simultaneously satisfied. We then store $\Delta m^{\text{uncompl}} = m_2 - m_i - \delta M_{\text{th}}$.

3. **Estimation**: This procedure is repeated 10^6 times. We then calculate β^{uncompl} and β^{compl} as the inverse of the mean values of $\Delta m^{\text{uncompl}}$ and Δm^{compl}, respectively.

Numerical results confirm that $\beta^{\text{uncompl}} = \beta$ within negligible statistical fluctuations. In Fig. 4, we plot the bias $\epsilon = (\beta^{\text{compl}}/\beta^{\text{uncompl}}) - 1$ as a function of $\delta M_{\text{th}}/\sigma$ for various values of β and σ. We observe a reasonable collapse of the curves when ϵ is scaled by $\beta^2\sigma^2$. The functional dependence is consistent with an exponential decay, well-approximated by the following expression:

$$\epsilon \simeq 0.2\,\beta^2\sigma^2 \left(\frac{\delta M_{\text{th}}}{\sigma} + 1\right) 10^{-\frac{\delta M_{\text{th}}}{\sigma}}. \qquad (13)$$

This result demonstrates that the bias caused by a finite σ becomes negligible ($\epsilon \lesssim 0.01$) as soon as $\delta M_{\text{th}} \gtrsim 2\sigma$.

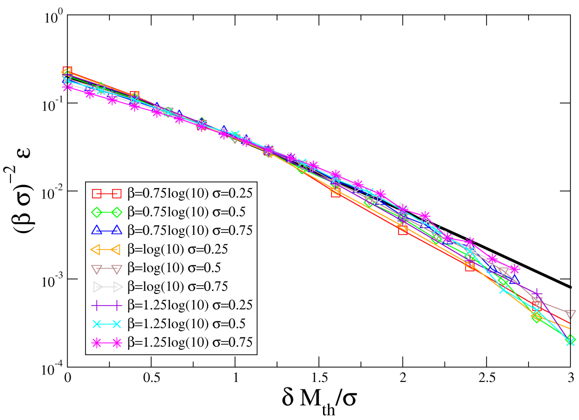

Figure 4 The estimated value of ϵ from numerical simulations plotted against $\delta M_{\text{th}}/\sigma$. We utilize a detection function given by Eq. (3) and magnitudes extracted from the GR law (Eq. 1). Different curves and symbols correspond to varying values of β and σ. The solid black curve represents the fit using Eq. (13).

Appendix B: How to correct magnitude rounding

Magnitudes in seismic catalogs are typically rounded to the first decimal digit. This rounding introduces a systematic bias in the estimate of the b-value through Eq. (5). This problem was first highlighted by UTSU (1966), who proposed an approximate correction to Eq. (2) for the evaluation of the b-value using the traditional method.

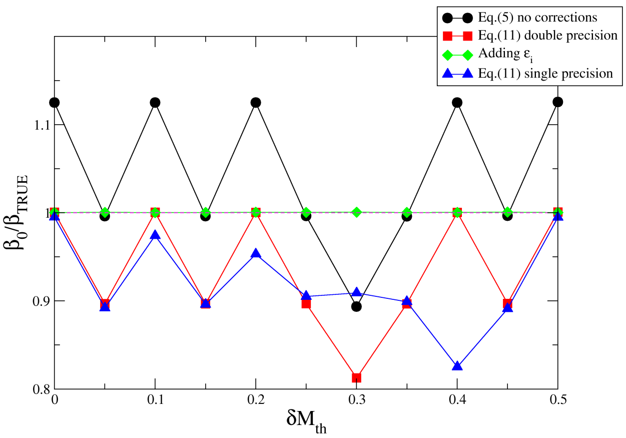

Figure 5 Estimated values of β_+ in a synthetic catalog with magnitudes rounded at $\Delta = 0.1$, for different values of δM_{th}. Black circles: results without rounding corrections. Red squares: Eq. (14) with double-precision arithmetic. Blue triangles: Eq. (14) with single-precision arithmetic. Green diamonds: Eq. (5) with random noise ϵ_i added to each m_i. The magenta dashed line indicates the true value $\beta_+ = \beta_{\text{TRUE}}$.

The bias becomes even more relevant when estimating b-value via the b-positive or b-more-positive estimators. An analytical expression that accounts for the rounding step Δ was derived by van der Elst (2021) and later rederived by Gasperini and Tinti (2023):

$$\beta_+ = \frac{1}{2\Delta} \ln\left(\frac{|\Delta M| + 2\Delta}{|\Delta M|}\right), \qquad (14)$$

where

$$|\Delta M| = \frac{1}{N_+} \sum_{\substack{i=1 \\ m_j > m_i + \delta M_{\text{th}}}}^{N_+} (m_j - m_i - \delta M_{\text{th}}). \qquad (15)$$

However, the use of Eq. (14) can present technical issues. First, Eq. (14) is strictly valid only when δM_{th} is an integer multiple of the rounding step, i.e. $\delta M_{\text{th}} = k\Delta$. When this condition is not satisfied, the estimate of $|\Delta M|$ becomes biased, since rounding introduces a systematic gap in $m_j - m_i - \delta M_{\text{th}}$ that is not compensated by Eq. (14).

To illustrate this effect, we generated a synthetic catalog containing $N = 10^6$ earthquakes distributed according to the GR law with a true β value, β_{TRUE}. We then applied rounding with $\Delta = 0.1$ to the magnitudes and estimated β_+ using Eq. (14) for different values of δM_{th}. The results show that when $\delta M_{\text{th}} = k \cdot 0.1$, the correct β_{TRUE} is recovered. Conversely, a systematic underestimation is observed when $\delta M_{\text{th}} = k \cdot 0.1 + \delta_k$, with $\delta_k = 0.5$. For other choices of $\delta_k \in (0, 1)$, deviations from β_{TRUE} are also observed, but these vanish as $\delta_k \to 0$ or $\delta_k \to 1$.

It is also worth noting that the computation of β_+ via Eq. (14) is highly sensitive to numerical precision. In

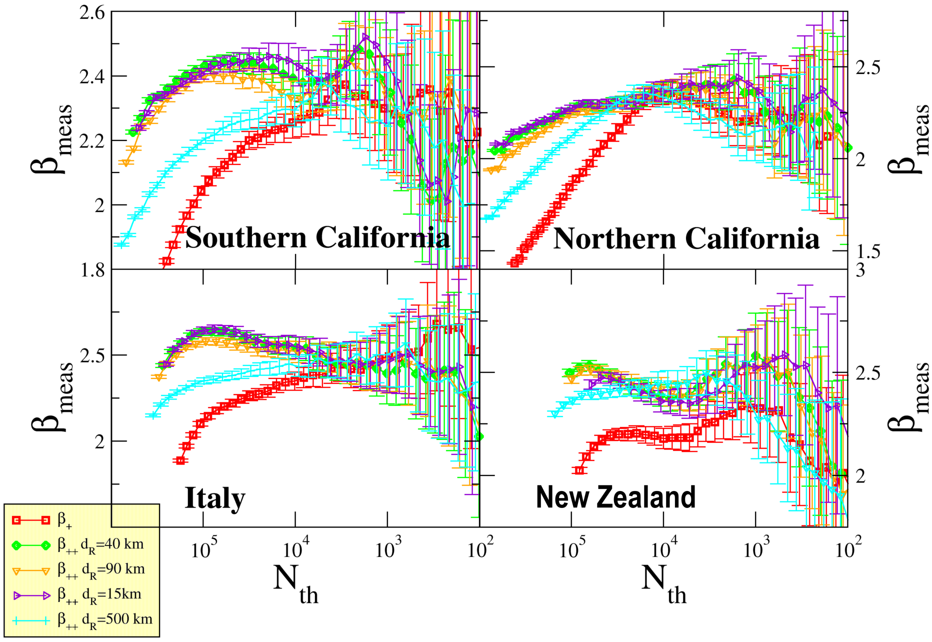

Figure 6 The values of β_+ and β_{++} (corresponding to $b = \beta/\ln(10)$), for different choices of d_R, are plotted as functions of N_{th} for the four geographic regions: Southern California (upper left), Northern California (upper right), Italy (lower left), and New Zealand (lower right).

Fig. 5, we show the results of Eq. (14) when $|\Delta M|$ is evaluated using single-precision floating-point arithmetic. In this case, a systematic underestimation occurs for all values of δM_{th}.

Conversely, we found that a stable estimate of β_+ can be obtained by correcting for rounding through the addition of a random noise term ϵ_i to each magnitude m_i in the catalog, where ϵ_i is drawn from a uniform distribution, $\epsilon_i \in (-0.5\Delta, 0.5\Delta)$. By applying this correction and directly using Eq. (5), we recover the correct β_{TRUE} for all values of δM_{th}, even under single-precision arithmetic (see Fig. 5). We remark that exactly the same behavior holds for the b-more positive estimator β_{++}. We have adopted both approaches in this study obtaining indistinguishable results, confirming that they are not affected by rounding problems.

Appendix C: Dependence on d_R

The b-more-positive estimator depends on the parameter, d_R, which represents the maximum distance between pairs included in the sum of Eq. (10). As discussed in Sec. 3.2, this constraint is required in order to satisfy Eq. (9). In Fig. 3, we have presented results for $d_R = 40\,\mathrm{km}$. Here we repeat the same analysis by exploring a broader range of values, $d_R \in [15\,\mathrm{km}, 500\,\mathrm{km}]$. The results indicate that for $d_R \lesssim 90\,\mathrm{km}$, the b-value estimate is only weakly affected by d_R, suggesting that Eq. (9) is reasonably satisfied. In contrast, for larger values of d_R, we observe significant deviations. A very similar behavior (not shown) is found for the Japan catalog.

Appendix D: Statistical test on the non-monotonicity of β_{++} in regional catalogs

The initial increase in β_{++} with δM_{th}, observed in all regional catalogs, aligns with theoretical predictions (Sec.3.2) and is indeed recovered in synthetic ETASI catalogs (Fig. 2). However, the subsequent decrease in β_{++}, which consistently appears in all but one instrumental catalog, was unexpected and may point to distinctive characteristics of real seismicity that are not fully captured by the ETASI model. This suggests that it is plausible that such behavior represents a genuine feature of real seismicity rather than a mere statistical fluctuation. To support this interpretation, we perform a test for correlated nested estimators (Cameron and Trivedi, 2005). Namely, we evaluate the quantity:

$$t = \frac{\beta_{++}^{\max} - \beta_{++}^{\min}}{\sqrt{\sigma_1^2 + \sigma_2^2 - 2r\sigma_1\sigma_2}}, \tag{16}$$

where σ_1 and σ_2 are the standard deviations of $\beta_{++}^{\max}$ and $\beta_{++}^{\min}$, respectively, and r is the correlation between $\beta_{++}^{\max}$ and $\beta_{++}^{\min}$ that can be estimated as

$$r \approx \sqrt{\frac{n}{n+m}}, \tag{17}$$

with n being the number of earthquakes used for estimating $\beta_{++}^{\max}$ and $n+m$ being the number of earthquakes used for estimating $\beta_{++}^{\min}$.

The values of $\beta_{++}^{\max}$, $\beta_{++}^{\min}$, σ_1, σ_2, and t are reported in Tab. 2. We find that the hypothesis of a significant decrease in β_{++}, corresponding to a significant difference between $\beta_{++}^{\max}$ and $\beta_{++}^{\min}$, can be accepted with a confidence level greater than 95 % for three regions (Japan, Italy, and New Zealand). For Southern California, the confidence level is about $90\,\%$, whereas for Northern California no evidence of a non-monotonic trend can be established.

Region	$\beta_{++}^{\max}$	σ_1	$\beta_{++}^{\min}$	σ_2	t	Significance level
Japan	2.104	0.0074	2.054	0.020	2.82	99%
South California	2.446	0.026	2.378	0.060	1.37	91%
North California	2.292	0.019	2.280	0.022	0.81	79%
Italy	2.636	0.021	2.550	0.057	1.84	95%
New Zealand	2.533	0.026	2.370	0.058	2.98	99%

Table 2 Statistical test comparing the maximum and minimum values of β_{++} ($\beta_{++}^{\max}$, $\beta_{++}^{\min}$), together with their standard deviations, the corresponding t-value, and the associated confidence level, in order to assess the non-monotonic behavior of β_{++} across the five geographic regions.

These results suggest that the non-monotonic behavior of β_{++} is a genuine pattern that is not fully captured by the ETASI model.

References

Aki, K. Maximum likelihood estimate of b in the formula $\log N = a - bM$ and its confidence limits. *Bulletin of the Earthquake Research Institute, University of Tokyo*, 43:237–239, 1965. doi: 10.15083/0000033631.

Cameron, A. C. and Trivedi, P. K. *Microeconometrics: methods and applications*. Cambridge university press, 2005. doi: 10.1017/CBO9780511811241.

Cao, A. and Gao, S. S. Temporal variation of seismic b-values beneath northeastern Japan island arc. *Geophysical Research Letters*, 29(9), May 2002. doi: 10.1029/2001gl013775.

de Arcangelis, L., Godano, C., Grasso, J. R., and Lippiello, E. Statistical physics approach to earthquake occurrence and forecasting. *Physics Reports*, 628:1–91, Apr. 2016. doi: 10.1016/j.physrep.2016.03.002.

de Arcangelis, L., Godano, C., and Lippiello, E. The Overlap of Aftershock Coda Waves and Short-Term Postseismic Forecasting. *Journal of Geophysical Research: Solid Earth*, 123(7), 2018. doi: 10.1029/2018jb015518.

Frohlich, C. and Davis, S. D. Teleseismic b values; Or, much ado about 1.0. *Journal of Geophysical Research: Solid Earth*, 98(B1): 631–644, Jan. 1993. doi: 10.1029/92jb01891.

Gasperini, P. and Tinti, S. The estimation of b-value of the frequency–magnitude distribution and of its 1 σ intervals from binned magnitude data. Apr. 2023. doi: 10.22541/essoar.168167163.30604759/v1.

Godano, C., Lippiello, E., and de Arcangelis, L. Variability of the b value in the Gutenberg–Richter distribution. *Geophysical Journal International*, 199(3):1765–1771, Oct. 2014. doi: 10.1093/gji/ggu359.

Godano, C., Petrillo, G., and Lippiello, E. Evaluating the incompleteness magnitude using an unbiased estimate of the b value. *Geophysical Journal International*, 236(2):994–1001, Dec. 2023. doi: 10.1093/gji/ggad466.

Godano, C., Tramelli, A., Petrillo, G., and Convertito, V. Testing the Predictive Power of b Value for Italian Seismicity. *Seismica*, 3(1), Feb. 2024. doi: 10.26443/seismica.v3i1.1084.

Godano, C., Lippiello, E., and Petrillo, G. Unsupervised Likelihood Inference of the b-Value via Magnitude Differences. *Journal of Geophysical Research: Machine Learning and Computation*, 2(4): e2025JH000863, 2025. doi: 10.1029/2025JH000863.

Gulia, L. and Wiemer, S. Real-time discrimination of earthquake foreshocks and aftershocks. Mar. 2020. doi: 10.5194/egusphere-egu2020-7590.

Gulia, L., Tormann, T., Wiemer, S., Herrmann, M., and Seif, S. Short-term probabilistic earthquake risk assessment considering time-dependent b values. *Geophysical Research Letters*, 43 (3):1100–1108, Feb. 2016. doi: 10.1002/2015gl066686.

Gulia, L., Wiemer, S., and Vannucci, G. Pseudoprospective Evaluation of the Foreshock Traffic-Light System in Ridgecrest and Implications for Aftershock Hazard Assessment. *Seismological Research Letters*, 91(5), 2020. doi: 10.1785/0220190307.

Gutenberg, B. and Richter, C. F. Frequency of earthquakes in California. *Bulletin of the Seismological Society of America*, 34(4): 185–188, Oct. 1944. doi: 10.1785/bssa0340040185.

Hainzl, S. Apparent triggering function of aftershocks resulting from rate–dependent incompleteness of earthquake catalogs. *Journal of Geophysical Research: Solid Earth*, 121(9), 2016a. doi: 10.1002/2016jb013319.

Hainzl, S. Rate-Dependent Incompleteness of Earthquake Catalogs. *Seismological Research Letters*, 87(2A):337–344, Feb. 2016b. doi: 10.1785/0220150211.

Hainzl, S. ETAS-Approach Accounting for Short-Term Incompleteness of Earthquake Catalogs. *Bulletin of the Seismological Society of America*, 112(1), 2021. doi: 10.1785/0120210146.

Hauksson, E., Yang, W., and Shearer, P. M. Waveform relocated earthquake catalog for southern California (1981 to June 2011). *Bulletin of the Seismological Society of America*, 102(5): 2239–2244, 2012. doi: 10.1785/0120120010.

Helmstetter, A., Kagan, Y. Y., and Jackson, D. D. Comparison of Short-Term and Time-Independent Earthquake Forecast Models for Southern California. *Bulletin of the Seismological Society of America*, 96(1):90–106, Feb. 2006. doi: 10.1785/0120050067.

Kagan, Y. Y. Short-Term Properties of Earthquake Catalogs and Models of Earthquake Source. *Bulletin of the Seismological Society of America*, 94(4):1207–1228, Aug. 2004. doi: 10.1785/012003098.

Lippiello, E. and Petrillo, G. b-more-incomplete and b-more positive: Insights on A Robust Estimator of Magnitude Distribution. Mar. 2023. doi: 10.22541/essoar.167870358.88587861/v1.

Lippiello, E., Godano, C., and de Arcangelis, L. Dynamical Scaling in Branching Models for Seismicity. *Physical Review Letters*, 98 (9), Feb. 2007. doi: 10.1103/physrevlett.98.098501.

Lippiello, E., de Arcangelis, L., and Godano, C. Influence of Time and Space Correlations on Earthquake Magnitude. *Physical Review Letters*, 100(3), Jan. 2008. doi: 10.1103/physrevlett.100.038501.

LIPPIELLO, E., DE ARCANGELIS, L., and GODANO, C. TIME, SPACE AND MAGNITUDE CORRELATIONS IN EARTHQUAKE OCCURRENCE. *International Journal of Modern Physics B*, 23(28n29): 5583–5596, Nov. 2009. doi: 10.1142/s0217979209063870.

Lippiello, E., Cirillo, A., Godano, G., Papadimitriou, E., and Karakostas, V. Real-time forecast of aftershocks from a single seismic station signal. *Geophysical Research Letters*, 43(12), 2016. doi: 10.1002/2016gl069748.

Lippiello, E., Petrillo, G., Godano, C., Tramelli, A., Papadimitriou, E., and Karakostas, V. Forecasting of the first hour aftershocks by means of the perceived magnitude. *Nature Communications*, 10(1), 2019. doi: 10.1038/s41467-019-10763-3.

Lippiello, E., de Arcangelis, L., and Godano, C. Positive Answer on the Existence of Correlations between Positive Earthquake Magnitude Differences. *Physical Review Letters*, 133(24), Dec. 2024. doi: 10.1103/physrevlett.133.244101.

Lippiello, E., Petrillo, G., Godano, C., and Dal Zilio, L. Toward Recognizing the Waveform of Foreshocks. *Geophysical Research Letters*, 52(15):e2025GL115466, 2025. doi: 10.1029/2025GL115466.

Lolli, B., Randazzo, D., Vannucci, G., and Gasperini, P. The Homogenized Instrumental Seismic Catalog (HORUS) of Italy from 1960 to Present. *Seismological Research Letters*, 91(6), 2020. doi: 10.1785/0220200148.

Lombardi, A. M. and Marzocchi, W. The ETAS model for daily forecasting of Italian seismicity in the CSEP experiment. *Annals of Geophysics*, 53(3):155–164, Nov. 2010. doi: 10.4401/ag-4848.

Mignan, A. and Woessner, J. Estimating the magnitude of completeness for earthquake catalogs. 2012. doi: 10.5078/CORSSA-00180805.

Mignan, A., Werner, M. J., Wiemer, S., Chen, C.-C., and Wu, Y.-M. Bayesian Estimation of the Spatially Varying Completeness Magnitude of Earthquake Catalogs. *Bulletin of the Seismological Society of America*, 101(3):1371–1385, May 2011. doi: 10.1785/0120100223.

Nandan, S., Ouillon, G., and Sornette, D. Magnitude of Earthquakes Controls the Size Distribution of Their Triggered Events. *Journal of Geophysical Research: Solid Earth*, 124(3):2762–2780, Mar. 2019. doi: 10.1029/2018jb017118.

Nandan, S., Ouillon, G., and Sornette, D. Are large earthquakes preferentially triggered by other large events? Mar. 2022. doi: 10.1002/essoar.10510831.1.

Ogata, Y. On Lewis Simulation Method for Point Processes. *IEEE*, 27(1):23, 1981. doi: 10.1109/TIT.1981.1056305.

Ogata, Y. Statistical Models for Earthquake Occurrences and Residual Analysis for Point Processes. *Journal of the American Statistical Association*, 83(401):9–27, Mar. 1988. doi: 10.1080/01621459.1988.10478560.

Ogata, Y. A Monte Carlo method for high dimensional integration. *Numerische Mathematik*, 55(2):137–157, Mar. 1989. doi: 10.1007/bf01406511.

Ogata, Y. Space-Time Point-Process Models for Earthquake Occurrences. *Annals of the Institute of Statistical Mathematics*, 50(2), 1998. doi: 10.1023/a:1003403601725.

Ogata, Y. and Katsura, K. Analysis of temporal and spatial heterogeneity of magnitude frequency distribution inferred from earthquake catalogues. *Geophysical Journal International*, 113 (3), 1993. doi: 10.1111/j.1365-246x.1993.tb04663.x.

Omori, F. On the after-shocks of earthquakes. *J. Coll. Sci. Imp. Univ. Tokyo*, 7:111–200, 1894. url={https://books.google.com/books?id=HtsPAAAAIAAJ}.

Peng, Z., Vidale, J. E., Ishii, M., and Helmstetter, A. Seismicity rate immediately before and after main shock rupture from high-frequency waveforms in Japan. *Journal of Geophysical Research: Solid Earth*, 112(B3), Mar. 2007. doi: 10.1029/2006jb004386.

Petrillo, G. and Lippiello, E. Testing of the foreshock hypothesis within an epidemic like description of seismicity. *Geophysical Journal International*, 225(2):1236–1257, Dec. 2020. doi: 10.1093/gji/ggaa611.

Petrillo, G. and Lippiello, E. Incorporating Foreshocks in an Epidemic-like Description of Seismic Occurrence in Italy. *Applied Sciences*, 13(8):4891, Apr. 2023. doi: 10.3390/app13084891.

Petrillo, G. and Zhuang, J. The debate on the earthquake magnitude correlations: A meta-analysis. Aug. 2022. doi: 10.21203/rs.3.rs-1984394/v1.

Petrillo, G. and Zhuang, J. Verifying the Magnitude Dependence in Earthquake Occurrence. *Physical Review Letters*, 131(15), Oct. 2023. doi: 10.1103/physrevlett.131.154101.

Petrillo, G., Landes, F., Lippiello, E., and Rosso, A. The influence of the brittle-ductile transition zone on aftershock and foreshock occurrence. Mar. 2020. doi: 10.5194/egusphere-egu2020-4676.

Petruccelli, A., Vannucci, G., Lolli, B., and Gasperini, P. Harmonic Fluctuation of the Slope of the Frequency–Magnitude Distribution (b-Value) as a Function of the Angle of Rake. *Bulletin of the Seismological Society of America*, 108(4), 2018. doi: 10.1785/0120170328.

Scholz, C. H. On the stress dependence of the earthquake b value. *Geophysical Research Letters*, 42(5):1399–1402, Mar. 2015. doi: 10.1002/2014gl062863.

Schorlemmer, D. and Woessner, J. Probability of Detecting an Earthquake. *Bulletin of the Seismological Society of America*, 98 (5):2103–2117, Oct. 2008. doi: 10.1785/0120070105.

Schorlemmer, D., Wiemer, S., and Wyss, M. Earthquake statistics at Parkfield: 1. Stationarity of b values. *Journal of Geophysical Research: Solid Earth*, 109(B12), Dec. 2004. doi: 10.1029/2004jb003234.

Spada, M., Tormann, T., Wiemer, S., and Enescu, B. Generic dependence of the frequency-size distribution of earthquakes on depth and its relation to the strength profile of the crust. *Geophysical Research Letters*, 40(4):709–714, Feb. 2013. doi: 10.1029/2012gl054198.

Tinti, S. and Mulargia, F. Confidence intervals of b values for grouped magnitudes. *Bulletin of the Seismological Society of America*, 77(6):2125–2134, Dec. 1987. doi: 10.1785/bssa0770062125.

Tormann, T., Enescu, B., Woessner, J., and Wiemer, S. Randomness of megathrust earthquakes implied by rapid stress recovery after the Japan earthquake. *Nature Geoscience*, 8(2):152–158, Feb. 2015. doi: 10.1038/ngeo2343.

UTSU, T. A Statistical Significance Test of the Difference in b-value between Two Earthquake Groups. *Journal of Physics of the Earth*, 14(2):37–40, 1966. doi: 10.4294/jpe1952.14.37.

van der Elst, N. J. B-Positive: A Robust Estimator of Aftershock Magnitude Distribution in Transiently Incomplete Catalogs. *Journal of Geophysical Research: Solid Earth*, 126(2), Feb. 2021. doi: 10.1029/2020jb021027.

Waldhauser, F. and Schaff, D. P. Large-scale relocation of two decades of Northern California seismicity using cross-correlation and double-difference methods. *Journal of Geophysical Research: Solid Earth*, 113(B8), Aug. 2008. doi: 10.1029/2007jb005479.

Wiemer, S. and Wyss, M. Minimum Magnitude of Completeness in Earthquake Catalogs: Examples from Alaska, the Western United States, and Japan. *Bulletin of the Seismological Society of America*, 90(4):859–869, Aug. 2000. doi: 10.1785/0119990114.

Wiemer, S. and Wyss, M. *Mapping spatial variability of the frequency-magnitude distribution of earthquakes*, page 259–V. Elsevier, 2002. doi: 10.1016/s0065-2687(02)80007-3.

Woessner, J. and Wiemer, S. Assessing the Quality of Earthquake Catalogues: Estimating the Magnitude of Completeness and Its Uncertainty. *Bulletin of the Seismological Society of America*, 95 (2):684–698, Apr. 2005. doi: 10.1785/0120040007.

Zhuang, J. and Ogata, Y. Properties of the probability distribution associated with the largest event in an earthquake cluster and their implications to foreshocks. *Physical Review E*, 73(4), Apr.

2006. doi: 10.1103/physreve.73.046134.